

Optimization of Skanavi model and its application to high permittivity materials

Hao Luo(罗昊), Xinrui Qin(秦新瑞), Kejia Geng(耿可佳), Cuncun Kong(孔存存), and Pengfei Cheng(成鹏飞)
Citation: Chin. Phys. B, 2025, 34 (**1**): 017702. DOI: 10.1088/1674-1056/ad9ba0
What follows is a list of articles you may be interested in

Dielectric anisotropy in liquid crystal mixtures with nematic and smectic phases

Xing-Zhou Tang(汤星舟), Jia-Yao Ye(叶家耀), Zi-Ye Wang(王子烨), Hao-Yi Jiang(姜皓译), Xiao-Hu Shang(尚小虎), Zhao-Yan Yang(杨朝雁), and Bing-Xiang Li(李炳祥)
Chin. Phys. B, 2024, 33 (**8**): 087702. DOI: 10.1088/1674-1056/ad4cd7

Observing ferroelastic switching in $Hf_{0.5}Zr_{0.5}O_2$ thin film

Zhao Guan(关赵), Tao Wang(王陶), Yunzhe Zheng(郑赟喆), Yue Peng(彭悦), Luqi Wei(魏鹿奇), Yuke Zhang(张宇科), Abliz Mattursun(阿卜力孜 cdot 麦提图尔苏), Jiahao Huang(黄家豪), Wen-Yi Tong(童文旖), Genquan Han(韩根全), Binbin Chen(陈斌斌), Ping-Hua Xiang(向平华), Chun-Gang Duan(段纯刚), and Ni Zhong(钟妮)
Chin. Phys. B, 2024, 33 (**6**): 067701. DOI: 10.1088/1674-1056/ad362f

$BaTiO_3$/p-GaN/Au self-driven UV photodetector with bipolar photocurrent controlled by ferroelectric polarization

Wushuang Han(韩无双), Kewei Liu(刘可为), Jialin Yang(杨佳霖), Yongxue Zhu(朱勇学), Zhen Cheng(程祯), Xing Chen(陈星), Binghui Li(李炳辉), Lei Liu(刘雷), and Dezhen Shen(申德振)
Chin. Phys. B, 2024, 33 (**4**): 047701. DOI: 10.1088/1674-1056/ad2607

Impact of annealing temperature on the ferroelectric properties of $W/Hf_{0.5}Zr_{0.5}O_2/W$ capacitor

Dao Wang(王岛), Yan Zhang(张岩), Yongbin Guo(郭永斌), Zhenzhen Shang(尚真真), Fangjian Fu(符方健), and Xubing Lu(陆旭兵)
Chin. Phys. B, 2023, 32 (**9**): 097701. DOI: 10.1088/1674-1056/aca9c6

Charge trapping effect at the interface of ferroelectric/interlayer in the ferroelectric field effect transistor gate stack

Xiaoqing Sun(孙晓清), Hao Xu(徐昊), Junshuai Chai(柴俊帅), Xiaolei Wang(王晓磊), and Wenwu Wang(王文武)
Chin. Phys. B, 2023, 32 (**8**): 087701. DOI: 10.1088/1674-1056/acd524

Optimization of Skanavi model and its application to high permittivity materials

Hao Luo(罗昊), Xinrui Qin(秦新瑞), Kejia Geng(耿可佳), Cuncun Kong(孔存存), and Pengfei Cheng(成鹏飞)†

School of Science, Xi'an Polytechnic University, Xi'an 710048, *China*

(Received 6 September 2024; revised manuscript received 23 October 2024; accepted manuscript online 9 December 2024)

A novel method is introduced to optimize the traditional Skanavi model by decomposing the electric field of molecules into the electric field of ions and quantitatively describing the ionic-scale electric field by the structural coefficient of the effective electric field. Furthermore, the optimization of the Skanavi model is demonstrated and the ferroelectric phase transition of $BaTiO_3$ crystals is revealed by calculating the optical and static permittivities of $BaTiO_3$, $CaTiO_3$, and $SrTiO_3$ crystals and the structure coefficients of the effective electric field of BT crystals after Ti^{4+} displacement. This research compensates for the deficiencies of the traditional Skanavi model and refines the theoretical framework for analyzing dielectric properties in high permittivity materials.

Keywords: electric field, structural coefficient, permittivity, Skanavi model

PACS: 77.80.–e, 77.80.B–, 77.84.–s, 77.84.Bw

DOI: 10.1088/1674-1056/ad9ba0 **CSTR:** 32038.14.CPB.ad9ba0

1. Introduction

Perovskite materials with high permittivity are widely utilized across diverse fields due to their electrical characteristics. These materials, known for their excellent charge storage capacity and superior electrical insulation, are crucial in the development of capacitors, energy storage systems, high-performance electronics, wireless communications, microwave components, and sensor technologies.[1–5] Current research is mainly focused on experimental studies and first-principles calculations,[6] and there is still a research gap in the investigation of perovskite materials with high permittivity through the methods of classical dielectric theory.

For typical perovskites, the frame of the cell is built by A-site cations with larger ionic radii at the corners, while the functional structural unit of the octahedron is formed by the interaction between anion of oxygen at the face-center and B-site cations with smaller ionic radius at the center of the octahedron. It is well known that dielectric properties of perovskites are mainly defined by the polarizable unit of BO_6 octahedron, however, the interaction between oxygen and A-site ions is also important for ferroelectrics.

Extensive research has been carried out to reveal the relationship between the structure and properties of perovskites at different levels, such as macroscopic, mesoscopic, or microscopic. Although theoretically simulation based on first principles is a super and effective way to explore the interaction between ions by relative positions of ions in the cell, state density, bond characteristics, and so on, it is an indirect way to explain macroscopic dielectric properties which are the results of dipoles distribution. In fact, the Clausius equation and Lorentz electric field model have built the solid basis for classical dielectric physics, which solves the theoretical problem of the composition of an effective electric field and its influence on dielectric permittivity. As for certain dielectrics, different approximation methods have to be adopted to simplify the calculation. For dielectrics with high permittivity, the structural coefficient of the effective electric field (from now on referred to as the structural coefficient) is a reasonable and direct calculation method, which is provided by Skanavi based on the superposition of electric fields and the point dipole approximation. Nevertheless, the method is only accepted by very few researchers for some serious defects. In Skanavi's model, the effective electric field in a crystal is decomposed into molecule-like units, however, the variation of their geometric configurations with different chemical environments is ignored. At the same time, the structural coefficient is calculated by an electric field excited by ions, however, the effective electric field in a crystal is analyzed based on molecule-like units. The inconsistency of the model brings initial difficulties.

Within the framework of dielectric theory, which uses the superposition of electric fields, the polarization intensity of the dielectric material is denoted as

$$P = \sum_i N_i \alpha_i \boldsymbol{E}_i, \tag{1}$$

where α_i is the molecular polarizabilities, defined as the sum of the electronic displacement polarizabilities of all ions within a molecule and the ionic displacement polarizability of the molecule. N_i represents the number of molecules per unit volume, and $\boldsymbol{E}_i$ is the effective electric field experienced by the molecule.

†Corresponding author. E-mail: pfcheng@xpu.edu.cn

© 2025 Chinese Physical Society and IOP Publishing Ltd. All rights, including for text and data mining, AI training, and similar technologies, are reserved.

The relationship between the polarization intensity P and the permittivity ε is given by

$$P = \varepsilon_0 (\varepsilon - 1) \boldsymbol{E}, \tag{2}$$

where ε_0 is the permittivity of vacuum, $\varepsilon_0 \approx 8.85418 \times 10^{-12}$ F/m, and $\boldsymbol{E}$ is the external electric field. Combining Eqs. (1) and (2) yields the Clausius equation

$$\varepsilon = \sum_i \frac{N_i \alpha_i \boldsymbol{E}_i}{\varepsilon_0 \boldsymbol{E}} + 1. \tag{3}$$

In general, the effective electric field and the external electric field are not equal, except for gas where the pressure is not too much. Therefore, to obtain the permittivity from the Clausius equation, the key problem is to find out the effective electric field acting on the molecule. Lorentz first proposed a theoretical model about the effective electric field, as seen in Fig. 1. A dielectric is sandwiched between the plates of a parallel-plate capacitor, and the molecule of interest, designated as O, is located at the center of a sphere with a radius of a. The radius of the sphere is much larger than the distance between molecules, allowing the region outside the sphere to be considered as a continuous medium. Consequently, the polarization effects of the molecules outside the sphere can be addressed using a macroscopic approach. Conversely, the sphere's radius is much smaller than the distance between the capacitor plates, ensuring that the electric field both inside and outside the sphere can be considered approximately constant. The interactions of other polarized molecules within the sphere on molecule O must account for the material structure of the dielectric. Utilizing the superposition of electric fields, Lorentz's effective electric field acting on the molecule O can be expressed as

$$\boldsymbol{E}_\mathrm{i} = \boldsymbol{E} + \boldsymbol{E}_1' + \boldsymbol{E}_2, \tag{4}$$

where $\boldsymbol{E}_1'$ represents the electric field produced by bound charges on the spherical cavity surface, and $\boldsymbol{E}_2$ is the electric field produced by all polarized molecules in the sphere except for the molecule O. Among them, $\boldsymbol{E}$ can be regarded as constant, and $\boldsymbol{E}_1'$ can use the superposition of electric fields to get $\boldsymbol{E}_1' = P/3\varepsilon_0$. Different treatments of $\boldsymbol{E}_2$ lead to different simplified models.

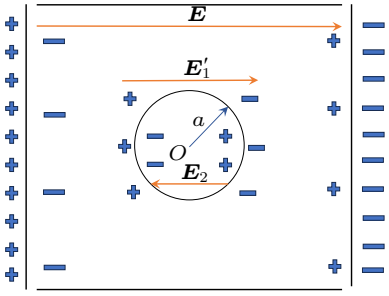


Fig. 1. The Lorentz electric field model.

Mossotti proposed that in nonpolar and weakly polar liquid dielectrics, their molecules induce dipole moments of equal magnitude when subjected to an electric field, with these dipole moments aligning along the electric field direction. Due to the amorphous nature of liquids, the likelihood of molecular presence is uniform. Therefore, the distribution of molecules within the Lorentz sphere can be regarded as symmetrical. In this context, the influence of the molecules inside the sphere on the molecule O's electric field can be neglected. The Mossotti's effective electric field can be expressed as

$$\boldsymbol{E}_\mathrm{i} = \boldsymbol{E} + \boldsymbol{E}_1'. \tag{5}$$

By substituting Eq. (5) into the Clausius equation, the classical Clausius–Mossotti equation (from now on referred to as the CM equation) is obtained[7]

$$\frac{\varepsilon - 1}{\varepsilon + 2} = \frac{N_\mathrm{i} \alpha_\mathrm{i}}{3\varepsilon_0}. \tag{6}$$

The above equation reveals that the CM equation neglects the influence of molecules within the sphere.

Furthermore, the Born model's approach to the effective electric field is somewhat rudimentary, treating the effective electric field inside the crystal as equivalent to the external electric field. Consequently, the polarization intensity can be expressed as

$$P = N (\alpha_\mathrm{e} + \alpha_\mathrm{a}) \boldsymbol{E}, \tag{7}$$

where α_e is the electronic displacement polarizability, and α_a is the ionic displacement polarizability. The dielectric polarizability α_d mentioned later can be obtained by summing electronic displacement polarizability and ionic displacement polarizability. Specific values for these polarizabilities will be provided later. Substituting Eq. (7) into Eq. (2) yields the Born formula

$$\varepsilon = 1 + \frac{N (\alpha_\mathrm{e} + \alpha_\mathrm{a})}{\varepsilon_0}. \tag{8}$$

By examining Eqs. (6) and (8), it is evident that these models introduce significant omissions in estimating the effective electric field. Therefore, the permittivities derived from the CM equation and the Born formula closely approximate the experimental values for ionic crystals with low permittivity. However, these models exhibit substantial errors for crystals with high permittivity. To address this, the Russian scientist Skanavi calculated the intensity of the electric field generated by the induced dipole moment of molecules positioned at the center of a sphere. He based his model on the Lorentz electric field, using the point dipole moment to represent the ion's induced dipole moments within the sphere under the electric field's influence. To differentiate the electric fields generated by ions of varying classes or positions within the sphere, Skanavi proposed the concept of the structural coefficient, which led to the development of a classical model for calculating the effective electric field. Although the Skanavi

model offers a more comprehensive approach to considering the effective electric field, it still has limitations in calculating the static permittivity of complex crystals with high permittivity:

(i) Calculating the static permittivity involves accounting for both the ionic displacement polarizabilities of the molecules and the electronic displacement polarizabilities of each ion. The electronic displacement polarizabilities of the ions can be determined using the formula mentioned later in the text. In diatomic molecules, the ionic displacement polarizabilities of the molecules are expressed through the elastic coefficient k for a pair of ions:

$$\alpha_{\mathrm{a}} = \frac{2q^2}{k}, \tag{9}$$

Here, q denotes the charge of the ions. The elastic coefficient k can be related to the intrinsic vibrational frequency f of the lattice ions:

$$w = 2\pi f = \sqrt{\frac{k}{m}}, \tag{10}$$

where m and w denote the reduced mass and angular frequency of diatomic molecules, respectively. However, there is a lack of comprehensive experimental data, with only limited values available for the intrinsic vibrational frequencies of simple diatomic molecular crystals. Furthermore, equation (9) does not apply to crystals composed of three or more elements.

(ii) In dielectric theory, the calculation of ionic displacement polarizability is conducted on a molecule basis. However, the effective electric field experienced by each ion within a molecule is generally non-uniform, which introduces errors related to converting or averaging the effective electric fields of individual ions. Moreover, even for molecules with identical elemental compositions, the effective electric field can differ depending on the crystal structure. For instance, the ionic displacement polarizability of TiO_2 molecules in the rutile phase may introduce significant inaccuracies when calculating the dielectric properties of the anatase or brookite phases. This is caused by variations in bond lengths, bonding characteristics, and structural distortions.

(iii) In 1948, Dutch physicist Van Santen[8] derived a formula for calculating the optical permittivity of cubic phase $BaTiO_3$ crystals using the classical Lorentz–Lorenz formula within the framework of the Skanavi model. However, specific values for the optical permittivity were not provided.

In this paper, we propose the method of decomposing the electric field of molecules into the electric field of ions and obtain the optical and static permittivity of typical perovskite crystals ($BaTiO_3$ (BT), $CaTiO_3$ (CT), and $SrTiO_3$ (ST)) by the structural coefficients that uncover the quantitative relationship of the electric fields between ions. The theoretically calculated values are in good agreement with the experimental values, especially significantly closer to the experimental values than those of the conventional CM equation and Born model. Moreover, the origin of the high permittivity of typical perovskite is revealed from the perspective of the variation of the structural coefficients and effective electric fields, which explains the microscopic mechanism of the displacement-type ferroelectric phase transition. This research addresses the limitations of the traditional Skanavi model, broadens the scope of its applicability, and advances the theoretical framework for the investigation of the dielectric properties of ionic crystals with high permittivities.

2. Computational methods

2.1. Optical permittivity

From the additivity rule of dielectric theory,[9–11] in ABO_3-type perovskite crystals, we can decompose the effective electric field of the ABO_3 molecule ($\boldsymbol{E}_{\mathrm{i}}$) into the effective electric fields of A^{2+}, B^{4+}, O_3^{2-}, and O_4^{2-} ($\boldsymbol{E}_{\mathrm{i1}}$, $\boldsymbol{E}_{\mathrm{i2}}$, $\boldsymbol{E}_{\mathrm{i3}}$, $\boldsymbol{E}_{\mathrm{i4}}$), and then the principle of additivity can be expanded by Eq. (1) as follows:

$$P = N\left(\alpha_{\mathrm{e1}}\boldsymbol{E}_{\mathrm{i1}} + \alpha_{\mathrm{e2}}\boldsymbol{E}_{\mathrm{i2}} + \alpha_{\mathrm{e3}}\boldsymbol{E}_{\mathrm{i3}} + 2\alpha_{\mathrm{e3}}\boldsymbol{E}_{\mathrm{i4}}\right). \tag{11}$$

Equation (11) involves α_{e1}, α_{e2}, and α_{e3}, which represent the electronic displacement polarizabilities of A^{2+}, B^{4+}, O_3^{2-}, and O_4^{2-}, where O_3^{2-} and O_4^{2-} share α_{e3}, as the electronic displacement polarizability. Furthermore, the effective electric fields of A^{2+}, B^{4+}, O_3^{2-}, and O_4^{2-} can be expressed respectively as follows:

$$\begin{aligned}\boldsymbol{E}_{\mathrm{i1}} &= \boldsymbol{E} + \frac{P}{3\varepsilon_0} + \alpha_{\mathrm{e1}}C_{11}\boldsymbol{E}_{\mathrm{i1}} + \alpha_{\mathrm{e2}}C_{12}\boldsymbol{E}_{\mathrm{i2}} + \alpha_{\mathrm{e3}}C_{13}\boldsymbol{E}_{\mathrm{i3}} \\ &\quad + \alpha_{\mathrm{e3}}C_{14}\boldsymbol{E}_{\mathrm{i4}}, \end{aligned} \tag{12}$$

$$\begin{aligned}\boldsymbol{E}_{\mathrm{i2}} &= \boldsymbol{E} + \frac{P}{3\varepsilon_0} + \alpha_{\mathrm{e1}}C_{21}\boldsymbol{E}_{\mathrm{i1}} + \alpha_{\mathrm{e2}}C_{22}\boldsymbol{E}_{\mathrm{i2}} + \alpha_{\mathrm{e3}}C_{23}\boldsymbol{E}_{\mathrm{i3}} \\ &\quad + \alpha_{\mathrm{e3}}C_{24}\boldsymbol{E}_{\mathrm{i4}}, \end{aligned} \tag{13}$$

$$\begin{aligned}\boldsymbol{E}_{\mathrm{i3}} &= \boldsymbol{E} + \frac{P}{3\varepsilon_0} + \alpha_{\mathrm{e1}}C_{31}\boldsymbol{E}_{\mathrm{i1}} + \alpha_{\mathrm{e2}}C_{32}\boldsymbol{E}_{\mathrm{i2}} + \alpha_{\mathrm{e3}}C_{33}\boldsymbol{E}_{\mathrm{i3}} \\ &\quad + \alpha_{\mathrm{e3}}C_{34}\boldsymbol{E}_{\mathrm{i4}}, \end{aligned} \tag{14}$$

$$\begin{aligned}\boldsymbol{E}_{\mathrm{i4}} &= \boldsymbol{E} + \frac{P}{3\varepsilon_0} + \alpha_{\mathrm{e1}}C_{41}\boldsymbol{E}_{\mathrm{i1}} + \alpha_{\mathrm{e2}}C_{42}\boldsymbol{E}_{\mathrm{i2}} + \alpha_{\mathrm{e3}}C_{43}\boldsymbol{E}_{\mathrm{i3}} \\ &\quad + \alpha_{\mathrm{e3}}C_{44}\boldsymbol{E}_{\mathrm{i4}}, \end{aligned} \tag{15}$$

Here, C_{AA} denotes the structural coefficients for ions of the same type, while C_{AB} indicates the structural coefficients for ions of different types. In C_{AA} and C_{AB}, the first subscript identifies the central ion and the second subscript identifies the surrounding ion, with subscripts 1, 2, 3, and 4 corresponding to A^{2+}, B^{4+}, O_3^{2-}, and O_4^{2-}, respectively. Then replacing the permittivity ε in Eq. (1) with the optical permittivity ε_∞, we get

$$P = \varepsilon_0\left(\varepsilon_\infty - 1\right)\boldsymbol{E}. \tag{16}$$

The optical permittivity of ABO_3-type perovskite crystals under the Skanavi model can be determined by combining Eqs. (11)–(16):

$$\frac{\varepsilon_\infty-1}{\varepsilon_\infty+2}=\frac{N}{3\varepsilon_0}\frac{\alpha_{e1}+\alpha_{e2}+3\alpha_{e3}+\alpha_{e3}(\alpha_{e1}C_{31}+\alpha_{e2}C_{32}+\alpha_{e3}C_{34}}{1-C_{11}\alpha_{e1}-C_{22}\alpha_{e2}-C_{33}\alpha_{e3}-C_{44}\alpha_{e3}-\alpha_{e3}\alpha_{e1}(C_{13}C_{31}+C_{14}C_{41})}\\ \frac{+2\alpha_{e1}C_{41}+2\alpha_{e2}C_{42}+2\alpha_{e3}C_{43})-C_{44}\alpha_{e3}(\alpha_{e1}+\alpha_{e2}+\alpha_{e3})+\Theta(\alpha_e^p)}{-\alpha_{e3}\alpha_{e2}(C_{23}C_{32}+C_{24}C_{42})-\alpha_{e3}^2C_{34}C_{42}}, \tag{17}$$

where the notation $\Theta(\alpha_e^p)$ denotes the multiple products of these electronic displacement polarizabilities. The structural coefficients are calculated using the following formulas:

$$C_{AA}=\frac{1}{4\pi\varepsilon_0}\cdot\sum_{j=1}^{N_A}\frac{2z_j^2-\left(x_j^2+y_j^2\right)}{\left(x_j^2+y_j^2+z_j^2\right)^{5/2}}, \tag{18}$$

$$C_{AB}=\frac{1}{4\pi\varepsilon_0}\cdot\sum_{j=1}^{N_B}\frac{2z_j^2-\left(x_j^2+y_j^2\right)}{\left(x_j^2+y_j^2+z_j^2\right)^{5/2}}, \tag{19}$$

where x_j, y_j, and z_j represent the coordinates of the surrounding ions j relative to the central ion. $N_{A/B}$ denotes the number of ions of the same class or different class compared to the ion of interest at the O point within the sphere.

2.2. Static permittivity

This paper transitions from focusing on finding or calculating the ionic displacement polarizabilities of molecules to calculating the ratio of the effective electric field to the external electric field $\boldsymbol{E}_i/\boldsymbol{E}$ (from now on referred to as the effective electric field ratio) starting from the Clausius equation. For example, in the case of the BT crystal, the effective electric field ratio $\boldsymbol{E}_i/\boldsymbol{E}$ for a single BT molecule can be decomposed into: the effective electric field ratio of one Ba^{2+} (denoted as $\boldsymbol{E}_{i1}/\boldsymbol{E}$), one Ti^{4+} (denoted as $\boldsymbol{E}_{i2}/\boldsymbol{E}$), one O_3^{2-} (denoted as $\boldsymbol{E}_{i3}/\boldsymbol{E}$), and two O_4^{2-} (denoted as $\boldsymbol{E}_{i4}/\boldsymbol{E}$). Furthermore, replace ε with ε_s and α_i with α_d in Eq. (3) to obtain

$$\varepsilon_s=\frac{N}{\varepsilon_0}\left[\alpha_{d1}\frac{\boldsymbol{E}_{i1}}{\boldsymbol{E}}+\alpha_{d2}\frac{\boldsymbol{E}_{i2}}{\boldsymbol{E}}+\alpha_{d3}\frac{\boldsymbol{E}_{i3}}{\boldsymbol{E}}+2\alpha_{d3}\frac{\boldsymbol{E}_{i4}}{\boldsymbol{E}}\right]+1. \tag{20}$$

To further determine the effective electric field ratios of the ions in Eq. (20), the first two terms on the right-hand side of Eqs. (12)–(15) need to be combined first to obtain

$$\boldsymbol{E}_{i1}=\frac{\varepsilon_\infty+2}{3}\boldsymbol{E}+\alpha_{e1}C_{11}\boldsymbol{E}_{i1}+\alpha_{e2}C_{12}\boldsymbol{E}_{i2}+\alpha_{e3}C_{13}\boldsymbol{E}_{i3}+\alpha_{e3}C_{14}\boldsymbol{E}_{i4}, \tag{21}$$

$$\boldsymbol{E}_{i2}=\frac{\varepsilon_\infty+2}{3}\boldsymbol{E}+\alpha_{e1}C_{21}\boldsymbol{E}_{i1}+\alpha_{e2}C_{22}\boldsymbol{E}_{i2}+\alpha_{e3}C_{23}\boldsymbol{E}_{i3}+\alpha_{e3}C_{24}\boldsymbol{E}_{i4}, \tag{22}$$

$$\boldsymbol{E}_{i3}=\frac{\varepsilon_\infty+2}{3}\boldsymbol{E}+\alpha_{e1}C_{31}\boldsymbol{E}_{i1}+\alpha_{e2}C_{32}\boldsymbol{E}_{i2}+\alpha_{e3}C_{33}\boldsymbol{E}_{i3}+\alpha_{e3}C_{34}\boldsymbol{E}_{i4}, \tag{23}$$

$$\boldsymbol{E}_{i4}=\frac{\varepsilon_\infty+2}{3}\boldsymbol{E}+\alpha_{e1}C_{41}\boldsymbol{E}_{i1}+\alpha_{e2}C_{42}\boldsymbol{E}_{i2}+\alpha_{e3}C_{43}\boldsymbol{E}_{i3}+\alpha_{e3}C_{44}\boldsymbol{E}_{i4}. \tag{24}$$

The mathematical transformation involves shifting the $\boldsymbol{E}_{i1}$, $\boldsymbol{E}_{i2}$, $\boldsymbol{E}_{i3}$, and $\boldsymbol{E}_{i4}$, from the left side of Eq. (21) through Eq. (24) to the right side. $(\varepsilon_\infty+2)\boldsymbol{E}/3$ is shifted to the left side, and then both sides are multiplied by $1/\boldsymbol{E}$ to obtain

$$-\frac{\varepsilon_\infty+2}{3}=(\alpha_{e1}C_{11}-1)\frac{\boldsymbol{E}_{i1}}{\boldsymbol{E}}+\alpha_{e2}C_{12}\frac{\boldsymbol{E}_{i2}}{\boldsymbol{E}}+\alpha_{e3}C_{13}\frac{\boldsymbol{E}_{i3}}{\boldsymbol{E}}+\alpha_{e3}C_{14}\frac{\boldsymbol{E}_{i4}}{\boldsymbol{E}}, \tag{25}$$

$$-\frac{\varepsilon_\infty+2}{3}=(\alpha_{e1}C_{21}-1)\frac{\boldsymbol{E}_{i1}}{\boldsymbol{E}}+\alpha_{e2}C_{22}\frac{\boldsymbol{E}_{i2}}{\boldsymbol{E}}+\alpha_{e3}C_{23}\frac{\boldsymbol{E}_{i3}}{\boldsymbol{E}}+\alpha_{e3}C_{24}\frac{\boldsymbol{E}_{i4}}{\boldsymbol{E}}, \tag{26}$$

$$-\frac{\varepsilon_\infty+2}{3}=(\alpha_{e1}C_{31}-1)\frac{\boldsymbol{E}_{i1}}{\boldsymbol{E}}+\alpha_{e2}C_{32}\frac{\boldsymbol{E}_{i2}}{\boldsymbol{E}}+\alpha_{e3}C_{33}\frac{\boldsymbol{E}_{i3}}{\boldsymbol{E}}+\alpha_{e3}C_{34}\frac{\boldsymbol{E}_{i4}}{\boldsymbol{E}}, \tag{27}$$

$$-\frac{\varepsilon_\infty+2}{3}=(\alpha_{e1}C_{41}-1)\frac{\boldsymbol{E}_{i1}}{\boldsymbol{E}}+\alpha_{e2}C_{42}\frac{\boldsymbol{E}_{i2}}{\boldsymbol{E}}+\alpha_{e3}C_{43}\frac{\boldsymbol{E}_{i3}}{\boldsymbol{E}}+\alpha_{e3}C_{44}\frac{\boldsymbol{E}_{i4}}{\boldsymbol{E}}. \tag{28}$$

By examining Eq. (25) through Eq. (28), the effective electric field ratio of each ion ($\boldsymbol{E}_{i1}/\boldsymbol{E}$, $\boldsymbol{E}_{i2}/\boldsymbol{E}$, $\boldsymbol{E}_{i3}/\boldsymbol{E}$, $\boldsymbol{E}_{i4}/\boldsymbol{E}$) can be determined when the optical permittivity, structural coefficients, and electronic displacement polarizabilities for the BT crystal are all known. Subsequently, the number of molecules per unit volume, the dielectric polarizabilities of each ion, the vacuum permittivity, and the effective electric field ratio of each ion can be substituted into Eq. (20) to calculate the static permittivity of the BT crystal. The same approach applies to determining the static permittivity of CT and ST crystals. Therefore, this paper will not detail it further.

In contrast to the traditional Skanavi model, the method described above addresses the limitations of Eq. (9) for complex crystals with high permittivity by employing the dielectric polarizabilities of individual ions. This approach not only resolves the applicability issues but also reduces errors associated with ionic displacement polarizabilities in molecules with identical elemental compositions across various crystal structures.

3. Polarizability

3.1. Electronic displacement polarizability

The isolated atom model is employed to calculate the electronic displacement polarizabilities of various ions in BT, CT, and ST crystals, as illustrated in Fig. 2. This model approximates the nucleus of an atom as a point charge with a charge of $+q$, while the total charge of the electrons outside the nucleus, $-q$, is modeled as a spherical electron cloud with

a uniform charge distribution. The center of this cloud is located at the nucleus, and its radius is a, as depicted in Fig. 2. When subjected to an external electric field $\boldsymbol{E}$, the electron cloud and the nucleus experience forces of equal magnitude but in opposite directions. This results in a displacement of the electron cloud relative to the nucleus, creating an induced dipole moment and thus electronic displacement polarization. According to the model, the electronic displacement polarizability α_e can be determined as follows:

$$\alpha_e = 4\pi\varepsilon_0 a^3. \tag{29}$$

The calculation of electronic displacement polarizability, α_e, as described in Eq. (29), requires knowledge of the ionic radius a. There are three primary types of ionic radius: (i) the Goldschmidt radius,[12] where ions are treated as rigid spheres, and the nearest-neighbor distances in ionic crystals are measured experimentally. The radii of other ions are inferred from empirical assumptions about the radii of the two most common negative ions (R (Cl) = 1.81 Å, R (O^{2-}) = 1.32 Å). (ii) The Shannon radius,[13] which is derived using a method similar to Goldschmidt's but accounts for the electronic spin state and the coordination of cations and anions. (iii) The Pauling radius,[14] where ions are considered as elastic spheres. In this method, the nearest-neighbor distance is determined when the Coulomb force between ions reaches equilibrium, and the derived radii are close to experimental values. The Pauling radius model treats ions as elastic spheres, considering the effect of overlapping electron clouds, which more accurately reflects the reality of ionic interactions. Therefore, this paper adopts the Pauling radius for calculations, with the specific values listed in the second column of Table 1. The calculated electronic displacement polarizabilities for a range of ions are detailed in Table 1. The values are expressed in the International System of Units (SI) within the third column and in the Gaussian System of Units (GS) within the fourth column.

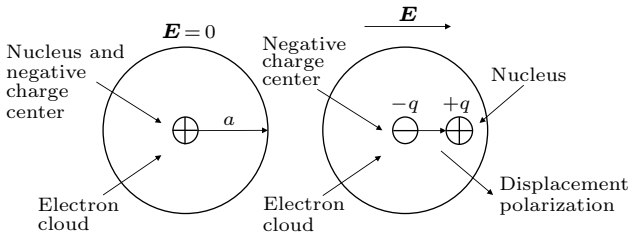


Fig. 2. The isolated atom model.

Table 1. Radii and electronic displacement polarizabilities.

Ions	a (Å)	$\alpha_e \times 10^{-40}$ (F·m^2)	α_e (Å^3)
Ba^{2+}	1.35	2.7375	2.4604
Ca^{2+}	0.99	1.0796	0.9703
Sr^{2+}	1.13	1.6054	1.4429
Ti^{4+}	0.68	0.3499	0.3144
O^{2-}	1.40	3.0531	2.7440

3.2. Ionic displacement polarizability and dielectric polarizability

According to the literature,[15] the permittivities calculated using the classical Roberts's ionic polarizabilities are in good agreement with experimental values, particularly for cubic phase perovskite crystals with high permittivities. This paper employs Roberts's ionic polarizabilities as the ionic displacement polarizabilities, as indicated in column 2 of Table 2. To facilitate the subsequent calculation of static permittivity for BT, CT, and ST crystals using the Skanavi model, it is necessary to account for both electronic and ionic displacement polarization simultaneously. The electronic displacement polarizabilities, based on the isolated atom model, are combined with Roberts's ionic displacement polarizabilities to derive the dielectric polarizabilities, as shown in column 3 of Table 2.

Table 2. Ionic displacement polarizability and dielectric polarizability.

Ions	α_a (Å^3)	α_d (Å^3)
Ba^{2+}	70.6	73.0604
Ca^{2+}	34.9	35.8703
Sr^{2+}	49.1	50.5429
Ti^{4+}	35.5	35.8144
O^{2-}	30.0	32.7440

4. Permittivities

4.1. Structural coefficients

Based on the Skanavi model and the unit cell structure of ABO_3-type crystals shown in Fig. 3, it is evident that BT, CT, and ST crystals contain four distinct classes of ions and 16 structural coefficients. These structural coefficients can be calculated from the crystal structures of BT, CT, and ST, with modeling conducted using Materials Studio software. This software exports CIF coordinate files for the $1 \times 1 \times 1$ cells of these crystals. The fractional coordinates of each ion were extracted from these CIF files and multiplied by the lattice constants of crystals to obtain the actual coordinates of each ion. These coordinates were then substituted into Eqs. (18) and (19) to calculate the structural coefficients, which are presented in Table 3. Additionally, Table 3 displays the measured lattice constants for cubic phase and tetragonal phase BT crystals. For cubic phase CT crystals, various scholars

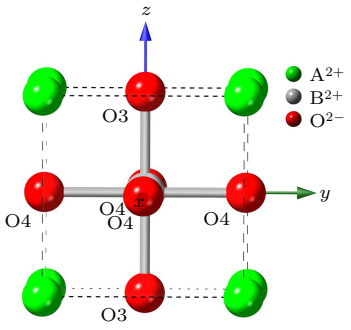


Fig. 3. ABO_3-type perovskite.

have reported different lattice constants. However, it is generally accepted that the lattice constants of the cubic phase CT crystals should fall within a specific range of 3.8 Å–3.9 Å. Kennedy[16] determined them to be $a = b = c = 3.8933$ Å at 1623 K, Lemanov[17] reported $a = b = c = 3.822$ Å, and Cockayne[18] provided $a = b = c = 3.8245$ Å. More recently, Rabiei[19] reported $a = b = c = 3.79 \pm 0.02$ Å. To minimize error in theoretical calculations, the average value within this range of 3.85 Å is used as the measured value for cubic phase CT. For cubic phase ST crystals, Abramov[20] obtained lattice constants of 3.8996 Å and 3.9011 Å at 145 K and 296 K, respectively, using high-precision single crystal x-ray diffraction. The lattice constant measured at 296 K is employed in this paper.

Table 3. Structural properties of BT, CT, and ST crystals.

Measured values of lattice constant of cubic phase BT[a)]	$a = 4$ Å	$b = 4$ Å	$c = 4$ Å	
Measured value of lattice constant of tetragonal phase BT[b)]	$a = 3.997$ Å	$b = 3.997$ Å	$c = 4.031$ Å	
Measured values of lattice constants of cubic phase CT	$a = 3.85$ Å	$b = 3.85$ Å	$c = 3.85$Å	
Measured values of lattice constants of cubic phase ST	$a = 3.9011$ Å	$b = 3.9011$ Å	$c = 3.9011$ Å	
Cubic phase BT ($C \times 10^{38}$)				
Ions	Ba^{2+}	Ti^{4+}	O_3^{2-}	O_4^{2-}
Ba^{2+}	$C_{11} = 0$	$C_{12} = 0$	$C_{13} = -6.2170$	$C_{14} = 6.2170$
Ti^{4+}	$C_{21} = 0$	$C_{22} = 0$	$C_{23} = 19.8769$	$C_{24} = -19.8169$
O_3^{2-}	$C_{31} = -6.2170$	$C_{32} = 19.8769$	$C_{33} = 0$	$C_{34} = 6.2170$
O_4^{2-}	$C_{41} = 3.1085$	$C_{42} = -9.9384$	$C_{43} = 3.1085$	$C_{44} = -6.2170$
Tetragonal phase BT ($C \times 10^{38}$)				
Ions	Ba^{2+}	Ti^{4+}	O_3^{2-}	O_4^{2-}
Ba^{2+}	$C_{11} = 0$	$C_{12} = 0$	$C_{13} = -6.0747$	$C_{14} = 6.0747$
Ti^{4+}	$C_{21} = 0$	$C_{22} = 0$	$C_{23} = 19.422$	$C_{24} = -19.442$
O_3^{2-}	$C_{31} = -6.0747$	$C_{32} = 19.442$	$C_{33} = 0$	$C_{34} = 6.0747$
O_4^{2-}	$C_{41} = 3.0376$	$C_{42} = -9.721$	$C_{43} = 3.0376$	$C_{44} = -6.0747$
Cubic phase CT ($C \times 10^{38}$)				
Ions	Ca^{2+}	Ti^{4+}	O_3^{2-}	O_4^{2-}
Ca^{2+}	$C_{11} = 0$	$C_{12} = 0$	$C_{13} = -6.8128$	$C_{14} = 6.8128$
Ti^{4+}	$C_{21} = 0$	$C_{22} = 0$	$C_{23} = 21.7817$	$C_{24} = -21.7817$
O_3^{2-}	$C_{31} = -6.8128$	$C_{32} = 21.7817$	$C_{33} = 0$	$C_{34} = 6.8128$
O_4^{2-}	$C_{41} = 3.40638$	$C_{42} = -10.902$	$C_{43} = 3.40638$	$C_{44} = -6.8128$
Cubic phase ST ($C \times 10^{38}$)				
Ions	Sr^{2+}	Ti^{4+}	O_3^{2-}	O_4^{2-}
Sr^{2+}	$C_{11} = 0$	$C_{12} = 0$	$C_{13} = -7.3443$	$C_{14} = 7.3443$
Ti^{4+}	$C_{21} = 0$	$C_{22} = 0$	$C_{23} = 23.4810$	$C_{24} = -23.4810$
O_3^{2-}	$C_{31} = -7.3443$	$C_{32} = 23.4810$	$C_{33} = 0$	$C_{34} = 7.3443$
O_4^{2-}	$C_{41} = 3.6721$	$C_{42} = -11.7526$	$C_{43} = 3.6721$	$C_{44} = -7.3443$

[a)]Ref. [21], [b)]Ref. [22].

(i) In the cubic phase of BT crystals, A-site ions are not easily displaced within the lattice due to their larger radius. Moreover, even if the structural coefficients for A-site ions are not negative, they remain relatively small and have a minimal impact on the crystal's permittivity. Therefore, these structural coefficients will not be further discussed. In contrast, the structural coefficient C_{32} is large and positive, indicating that Ti^{4+} is moved by the external electric field $\boldsymbol{E}$. This displacement enhances the O_3^{2-}'s effective electric field in the same direction, leading to significant distortion of the electron cloud around O_3^{2-}. Due to the unique crystal structure, the polarized O_3^{2-} yields a large positive structural coefficient for C_{23}, which further interacts with Ti^{4+}, intensifying the effective electric field on Ti^{4+} and leading to increased displacement of Ti^{4+}. Moreover, since C_{24} and C_{42} are both negative, the interaction between Ti^{4+} and O_4^{2-} should contribute to weakening the effective electric field. However, C_{42}, being a negative value with a large absolute value, indicates that the dipole moment formed after the displacement of Ti^{4+} significantly weakens the effective electric field acting O_4^{2-}. As a result, the electron cloud of O_4^{2-} undergoes almost no significant distortion. Even if C_{24} is also a negative number with a large absolute value, it does not reduce the effective electric field on Ti^{4+}. Therefore, the effective electric field of cubic phase BT crystals is framed by the mutually reinforcing interactions of Ti^{4+} and O_3^2, in which the high valence, small radius Ti^{4+} within the oxygen octahedral gap plays a key role.

(ii) In tetragonal phase BT crystals, although the structural coefficients C_{32} and C_{23} remain large positive values, they have decreased by 2% relative to those in cubic phase BT crystals. This decrease indicates a slight reduction in the mutual reinforcement between Ti^{4+} and O_3^2. Additionally, the abso-

lute value of C_{42} has decreased by 2%, and that of C_{24} has decreased by 1.8%, suggesting a diminished weakening effect between Ti^{4+} and O_4^{2-}.

(iii) In cubic phase CT crystals: the structural coefficients C_{32} and C_{23} are positive, while C_{24} and C_{42} are negative. This suggests that Ti^{4+} and O_3^{2-} are mutually reinforcing, whereas Ti^{4+} and O_4^{2-} are mutually weakening.

(iv) In cubic phase ST crystals: the structural coefficients C_{32} and C_{23} are the largest among all crystals, and C_{24} and C_{42} are the largest negative values compared to those in BT crystals. This indicates that the mutual reinforcement between Ti^{4+} and O_3^{2-} is stronger, while the mutual weakening between Ti^{4+} and O_4^{2-} is also more pronounced.

4.2. Optical permittivity of BT, CT, and ST crystals

The number of molecules per unit volume N is derived from the lattice constants of BT, CT, and ST crystals, as detailed in column 2 of Table 4. The structural coefficients for these crystals are obtained from Table 3. By substituting these values into Eq. (17), the optical permittivities for various crystals under the Skanavi model are calculated, as presented in column 4 of Table 4. Additionally, the optical permittivities under the Born formula and CM equation are shown in columns 5 and 6 of Table 4, respectively. The values in parentheses in Table 4 indicate the errors between the theoretical calculations and the experimental data.

Table 4. Optical permittivity.

Crystals	$N\times10^{28}$	Exp	Sk	Born	CM
Cubic BT	1.5625	5.40[a)]	5.60 (3%)	3.16 (41%)	8.70 (61%)
Tetragonal BT	1.5267	5.05[b)]	5.38 (6%)	3.11 (38%)	8.11 (60%)
Cubic CT	1.7523	5.81[c)]	5.12 (11%)	3.09 (46%)	7.95 (36%)
Cubic ST	1.6844	5.18[c)]	5.07 (2%)	3.12 (39%)	8.16 (57%)

[a)]Ref. [21], [b)]Ref. [23], [c)]Ref. [24].

The three approximation models, Skanavi, CM, and Born, employ different effective electric fields. The CM equation omits $\boldsymbol{E}_2$ from the Lorentz effective electric field, while the Born model excludes both $\boldsymbol{E}_1'$ and $\boldsymbol{E}_2$. In contrast, the Skanavi model includes all components of the Lorentz effective electric field. Therefore, the theoretical permittivity calculated using the Skanavi model should be the highest, the Born model should yield the lowest value, and the CM equation value should lie between those of the Skanavi and Born models. Unexpectedly, the results in Table 4 reveal that the permittivity calculated using the CM equation is higher than that of the Skanavi model and exceeds the experimental value. To research this discrepancy, we propose adjusting the CM equation (Eq. (6)) and the Skanavi model (Eq. (17)) by shifting the right side by '-1' on the left side and excluding higher-order polarizability terms that contribute minimally to optical permittivity. The revised results are as follows:

$$\varepsilon = \frac{N\alpha}{3\varepsilon_0}(\varepsilon+2)+1, \tag{30}$$

$$\varepsilon = \frac{N\alpha}{3\varepsilon_0}\cdot(\varepsilon+2)\cdot\frac{1}{1-C_{44}\alpha_{e3}}+1. \tag{31}$$

Upon examining Eqs. (30) and (31), it is evident that equation (30) does not include the term $1/(1-C_{44}\alpha_{e3})$ that is present in Eq. (31). According to Table 3, the C_{44} values for various crystals are all negative, which implies that $1/(1-C_{44}\alpha_{e3})$ is less than 1. Consequently, the optical permittivity calculated using the Skanavi model is smaller than the theoretical value calculated with the CM equation. The Skanavi model provides a more accurate estimate of high permittivity crystals, resulting in the smallest relative error for the optical permittivity. In contrast, the CM equation overestimates the influence of external molecules on the electric field at the center of the sphere, leading to the highest relative error in the optical permittivity.

4.3. Static permittivities of BT, CT, and ST crystals

Substituting the experimental values of the optical permittivity for each crystal, the structural coefficients, and the electronic displacement polarizabilities of each ion into Eqs. (25)–(28) yields the effective electric field ratios of ions, as presented in Table 5. These ratios, along with the dielectric polarizabilities and the number of molecules per unit volume, are substituted into Eq. (20) to calculate the static permittivities of BT, CT, and ST crystals using the Skanavi model, as presented in Table 5. Additionally, the static permittivities for various crystals calculated using the Born formula and the CM equation are also provided in Table 5. For the experimental value of static permittivities of cubic and tetragonal phase BT crystals, the static permittivity of the BT crystals away from the Curie point and at the relatively flat place of the curve in the graph of dielectric properties measured by Jonker[25] was chosen as the experimental value of static permittivity of BT crystals (Exp), as shown in Table 5. According to Lemanov[17] and Cockayne,[18] the static permittivity of CT crystals decreases with increasing temperature. At room temperature, the permittivity of orthorhombic CT crystals is noted as 170–190. Experimental results by Linz[26] also showed a significant negative correlation between the permittivity of CT crystals and temperature. Based on the trends observed in Linz's graphs, it is found that the permittivity of CT crystals at temperatures above 450 K is below 150. Accordingly, this paper adopts 150 as the experimental value for the permittivity of cubic phase CT crystals at high temperatures. For cubic phase ST crystals, the experimental permittivity at room temperature is taken as 275, as reported by Wainer.[27]

The static permittivity of cubic phase BT crystals calculated using the Skanavi model is larger than those of tetragonal phase BT crystals. This is in agreement with Jonker's experimental observations.[25] For CT and ST crystals, the Skanavi

model provides theoretical values that are closest to the experimental values. In contrast, the results from the Born formula and the CM equation exhibit substantial discrepancies from the experimental values and show opposite trends. This suggests that the Skanavi model more accurately captures the contribution of polarized molecules within the Lorentz sphere to the effective electric field and effectively accounts for the long-range coulombic interactions of dipole moments.

Table 5. The effective electric field ratios and static permittivities.

Dielectric properties	Cubic BT	Tetragonal BT	Cubic CT	Cubic ST
$\boldsymbol{E}_{i1}/\boldsymbol{E}$	2.4079	2.3188	2.5777	2.3486
$\boldsymbol{E}_{i2}/\boldsymbol{E}$	2.6559	2.5465	2.6838	2.5361
$\boldsymbol{E}_{i3}/\boldsymbol{E}$	2.6942	2.5860	2.6174	2.4020
$\boldsymbol{E}_{i4}/\boldsymbol{E}$	2.3830	2.2936	2.4959	2.2028
Sk	102	98	97.3927	93
Born	41	41.4	38.4167	40.1
CM	–2.3	–2.2	–2.2615	–2.2
Exp	1800	1200	150	275

The CM equation yields negative values because it is generally applicable to gas media with relatively low pressures, assuming the medium is uniform and isotropic, with no molecular interactions. This assumption effectively neglects the contribution of the second term, $\boldsymbol{E}_2$, in the Lorentz effective electric field. However, in BT, CT, and ST crystals, the molecular distance is much smaller compared to those in gases. Specifically, the number of molecules per unit volume in these crystals exceeds the number of molecules per unit volume in gases at standard conditions (2.687×10^{25} m^{-3}). The increased interaction between dipole molecules in these crystals means that ignoring E_2 leads to a situation where the term $N\alpha/\varepsilon$ in Eq. (6) is greater than '1', resulting in a permittivity of less than '1'.

The discrepancy between the theoretical values calculated by the Skanavi model and the experimental values can be attributed to the following factors: (i) the use of a unit cell in the calculation of structural coefficients, whereas a supercell should be used; (ii) the experimental values referenced may be affected by point defects in the sample and other external mechanisms. These factors will be deeply analyzed in further research.

The effective electric field within cubic BT crystals is established through the mutual reinforcement between Ti^{4+} and O_3^2. It would be expected that with larger structural coefficients C_{32} and C_{23}, the static permittivity would correspondingly increase. Paradoxically, in the cubic phases of BT, CT, and ST crystals, an increase in C_{32} and C_{23} is associated with a decrease in static permittivity. This phenomenon can be attributed to the increasing absolute value of the structural coefficient C_{31} within the cubic phase crystals, indicating an enhanced inhibitory effect of the A-site ions on the effective electric field of O_3^2, thereby leading to a reduction in the static permittivity. In summary, while the substantial positive values of C_{32} and C_{23} contribute to a higher static permittivity in cubic crystals, the presence of a small negative value for C_{31} results in a slight decrease in this permittivity.

In cubic phase crystals, there is a positive correlation between the effective electric field ratio of Ti^{4+} ($\boldsymbol{E}_{i2}/\boldsymbol{E}$) and the effective electric field ratio of O_3^2 ($\boldsymbol{E}_{i3}/\boldsymbol{E}$) with the static permittivity. This implies that an increase in the combined magnitude of $\boldsymbol{E}_{i2}/\boldsymbol{E}$ and $\boldsymbol{E}_{i3}/\boldsymbol{E}$ results in an enhancement of the static permittivity. Moreover, the effective electric field ratios of Ti^{4+} and O_3^2 are the highest among all such ratios. This underscores that the static permittivity of cubic phase crystals is predominantly influenced by the effective electric fields of Ti^{4+} and O_3^2.

5. Ti^{4+}'s displacement on BT crystals

5.1. Structural coefficients

When BT crystals transition from the paraelectric phase to the ferroelectric phase, Ti^{4+} displaces along the direction of the z-axis of the oxygen octahedron. Experimental measurements have determined that the average displacement of Ti^{4+} is 0.055 Å.[28] To investigate the impact of Ti^{4+} displacement on cubic and tetragonal phase BT crystals, simulations will be conducted under an electric field, maintaining a constant space group and lattice parameters. Subsequently, the structural coefficients of the displaced BT crystals will be analyzed. The specific procedure is as follows: Using Materials Studio software, Ti^{4+} will be displaced along the z-axis of the oxygen octahedron by three specified displacement values: 0.02 Å, 0.04 Å, and 0.055 Å. To minimize the number of variables in the calculations, O^{2-} will be constrained to the face centers as closely as possible. After modeling, CIF coordinate files for the corresponding unit cells will be exported. The fractional coordinates of each ion, derived from these files, are then multiplied by the lattice constants and used in Eqs. (18) and (19) to calculate the structural coefficients. The primary coefficients C_{23}, C_{32}, C_{24}, and C_{42} for cubic and tetragonal phase BT crystals at varying Ti^{4+} displacement levels are presented in Fig. 4.

In the cubic phase of BT crystals, the structural coefficients C_{32} and C_{23} exhibit identical values under the same displacement, and they decrease as the displacement of Ti^{4+} increases, hence they are represented by the same line. The absolute value of the structural coefficient C_{42} slightly increases with the displacement of Ti^{4+} increases, while the absolute value of C_{24} significantly increases with the displacement of Ti^{4+} increases. This indicates that these structural coefficients suppress the effective electric field of the cubic phase BT crystals, thereby inhibiting dielectric polarization. It also suggests that the cubic lattice is unfavorable to the displacement of Ti^{4+}.

Within the tetragonal phase of BT crystals, the structural coefficients C_{32} and C_{23} share identical values under the same

displacement, and they increase as the displacement of Ti^{4+} increases. Conversely, the structural coefficients C_{42} and C_{24} decrease as the displacement of Ti^{4+} increases. This indicates that these structural coefficients enhance the effective electric field of the tetragonal phase BT crystals, thereby promoting dielectric polarization. It also suggests that the tetragonal phase facilitates the displacement of Ti^{4+}, indicating the occurrence of a ferroelectric phase transition.

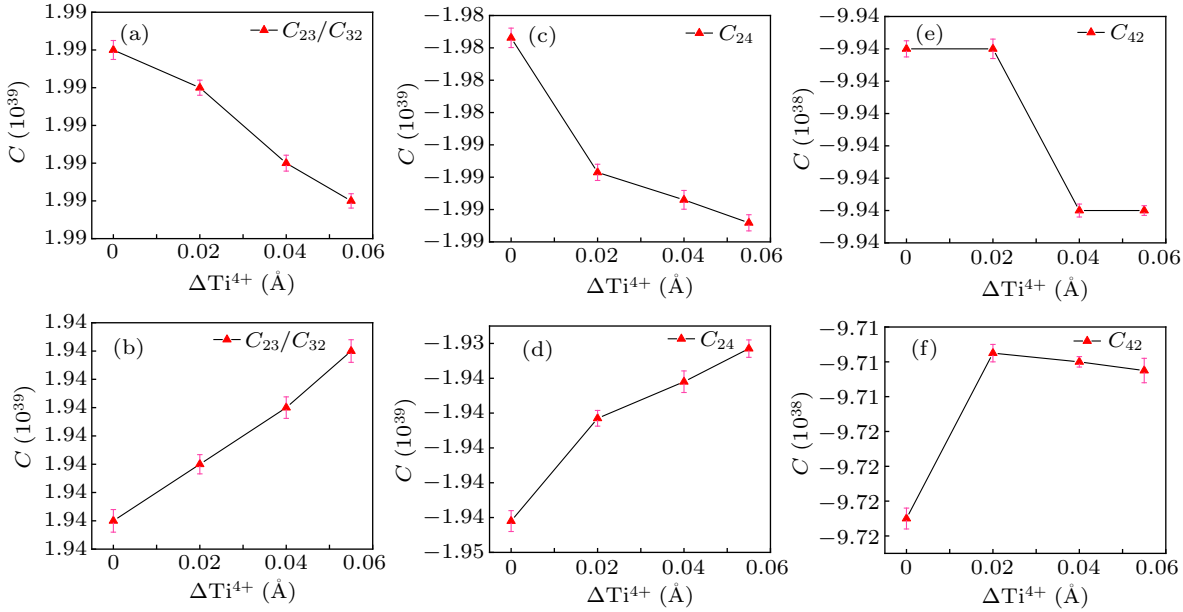


Fig. 4. (a) C_{32} and C_{23} for the cubic phase of BT. (b) C_{32} and C_{23} for the tetragonal phase of BT. (c) C_{24} for the cubic phase of BT. (d) C_{24} for the tetragonal phase of BT. (e) C_{42} for the cubic phase of BT. (f) C_{42} for the tetragonal phase of BT.

6. Conclusion

This study, utilizing the Skanavi model, the Clausius equation, the additivity rule, and the point dipole approximation, introduces a method for analyzing molecular electric fields by decomposing them into ionic electric fields. It quantifies the relationship between the electric field at the ionic level through structural coefficients and calculates the optical and static permittivities for BT, CT, and ST crystals. The results demonstrate that the theoretical predictions from the Skanavi model offer significant improvements over those from the CM equation and Born formula, aligning closely with experimental data. Furthermore, by examining the changes in structural coefficients before and after Ti^{4+} displacement along the z-axis, this paper elucidates the microscopic mechanisms underlying the ferroelectric phase transition in BT crystal. This research overcomes the limitations of the traditional Skanavi model and establishes a theoretical basis for calculating permittivities in complex crystals with high permittivity.

Acknowledgements

Project supported by the National Natural Science Foundation of China (Grant No. 51277138), the Natural Science Basic Research Program of Shaanxi Province of China (Grant No. 2021JM-442), and the Fund from the Shaanxi Provincial Science and Technology Department for Qin Chuangyuan Scientist + Engineer Team (Grant No. 2024QCY-KXJ-194).

References

[1] Adediji Y B, Adeyinka A M and Yahya D I 2023 *Energy Ecol Environ* **8** 401
[2] Szafraniak B, Fuśnik Ł, Xu J, *et al*. 2021 *Coatings* **11** 185
[3] Prasatkhetragarn A, Sareein T, Triamnak N, *et al*. 2022 *Ferroelectrics* **586** 224
[4] Ma J Y 2024 *Chin. Phys. Lett* **41** 078202
[5] Yao H B 2022 *Chin. Phys. B* **31** 088106
[6] Guo X, Li Y, Xiao W, *et al*. 2024 *Physica C* **617** 1354447
[7] Talebian E and Talebian M A 2013 *Optik* **124** 2324
[8] Van Santen J H and Opechowski W 1948 *Physica* **14** 545
[9] Shannon R D 1993 *J. Appl. Phys.* **73** 348
[10] Tessman J R, Kahn A H and Shockley W 1953 *Phys. Rev.* **92** 890
[11] Pirenne J and Kartheuser E 1964 *Physica* **30** 2005
[12] Goldschmidt V M 1929 *Trans. Faraday Soc.* **25** 253
[13] Shannon R D 1976 *Acta Cryst.* **32** 751
[14] Pauling L J 1927 *Am. Chem. Soc.* **49** 765
[15] Roberts S 1949 *Phys. Rev.* **76** 1215
[16] Kennedy B J, Howard C J and Chakoumakos B C 1999 *J. Phys.-Condens. Mat.* **11** 1479
[17] Lemanov V V, Sotnikov A V, Smirnova E P, *et al*. 1999 *Solid State Commun.* **110** 611
[18] Cockayne E and Burton B P 2000 *Phys. Rev. B* **62** 3735
[19] Rabiei M, Palevicius A, Monshi A, *et al*. 2020 *Nanomaterials-Basel* **10** 1627
[20] Abramov Y A, Tsirelson V G, Zavodnik V E, *et al*. 1995 *Acta Cryst.* **51** 942
[21] Ghosez P S H, Gonze X and Michenaud J P 1998 *Ferroelectrics* **206** 205
[22] Evarestov R A and Bandura A V 2012 *J. Comput. Chem.* **33** 1123
[23] Hermet P, Veithen M and Ghosez P 2009 *J. Phys.: Condens. Matter* **21** 215901
[24] Zhong W, King-Smith R D and Vanderbilt D 1994 *Phys. Rev. Lett.* **72** 3618
[25] Jonker G H and Van Santen J H 1949 *Science* **109** 632
[26] Linz Jr A and Herrington K 1958 *J. Chem. Phys.* **28** 824
[27] Wainer E 1946 *Trans. Electrochem. Soc.* **89** 331
[28] Shu H B, Zhou G C and Zhong X L, *et al*. 2007 *J. Phys.: Condens. Matter* **19** 276213